Journal of Environmental Science and Engineering B12 (2023) 265-279
doi:10.17265/2162-5263/2023.06.003

Modelling, Validation, and Calculations of Stratospheric Ozone Dynamics and Latitudinal Changes

Ibraheem Alelmi, Laurie Wei and Sen Nieh

Department of Mechanical Engineering, the Catholic University of America, Washington, DC 20064, U.S.A.

Abstract: This paper presents an engineering system approach of 2-D cylindrical model of mass balance calculations with convection, diffusion, and all potential photolysis, ozone generating and depleting chemical reactions considered. This model was developed, validated, and tested under different conditions for the stratospheric ozone. The calculated ozone concentrations and profile in the stratosphere at both the Equator and mid-latitudinal location of 40 °S were found to exhibit a similar and close profile and peak value of the published measured data. The discrepancy between the calculations and measurements for the average ozone concentration was shown to be less than 1% and the variation of distributions to be less than 19%. The latitudinal changes of ozone concentrations, distribution, and peak of the layer were found to shift from 9.41 ppm at mid-altitude of z = 30 km at the Equator, to 7.81 ppm at z = 34.5 km at 40 °S, to 5.78 ppm at higher altitude z = 39 km at the South Pole. The total ozone abundances at strategic latitudes at 0 °S, 20 °S, 40 °S, 60 °S, and 90 °S, were found to remain stable and not much changed, from 305 DU to 335 DU, except a smaller value of 288 DU at the South Pole. The possible explanations of ozone profile change and peak shifting as affected by solar/UV radiation, latitudinal locations, and ozone-depleting reactions were discussed and elaborated. The 2-D ozone Model presented in this paper is a robust, efficient, executable, and validated model for studying the complex ozone phenomena in the stratosphere.

Key words: 2-D ozone model, stratospheric ozone, validation, ozone depletion, latitudinal changes.

1. Introduction

The Earth's atmosphere extending from the sea level to about 300 km altitude in the upper sky is a multi-layered system crucial for supporting life, particularly the troposphere with most breathable air from ground to about 10-15 km altitude, the stratosphere with protective layers of ozone and greenhouse gases from 10-15 km to about 50 km altitude, and the remaining mesosphere and thermosphere. In the stratosphere, ozone O_3 molecules act as guardians, absorbing high energy UV (Ultraviolet) rays and safeguarding the overall surface of the planet. The Sun radiates infrared (heat), visible light, and invisible UV to Earth. There are three types of UV radiation: the higher-energy UV-C (100 to 280 nm wavelengths), the UV-B (280 to 315 nm), and the lower-energy UV-A (315to 400 nm), and collectively they amount to about 9% of the total solar energy.

Corresponding author: Sen Nieh, Ph.D., professor, research fields: combustion, energy and environment.

Exposure to the UV-C radiation is very dangerous to all life forms, which fortunately is entirely absorbed within the ozone layer of the stratosphere. Most UV-B radiation is absorbed by the ozone layer, which can cause skin cancer, cataracts, and suppressed immune system for humans. The UV-A radiation is mostly not absorbed by the ozone layer, which can cause aging of the skin if exposed to it for an extended period of time. The presence of ozone layer in the stratosphere functions as a natural sunscreen and absorbs about 90% of harmful UV rays and protects all living beings [1]. As for the total ozone in the atmosphere, a significant proportion (~90%) of it remains in the stratosphere as "good" protective ozone, while a smaller fraction (~10%) of it is found in the troposphere, particularly those near the ground, being regulated as a criterion pollutant, as "bad" photochemical smog ozone [1-3].

By the mid-1980s, scientists had discovered that there was an unusual thinning of the ozone layer over Antarctica. The discovery of this ozone hole caused a

major concern for the scientists and all governments in the world. They identified nearly 100 ODSs (Ozone Depletion Substances) that needed to be regulated in terms of their production and usage to reduce the depletion of the stratospheric ozone. ODSs can be grouped into three types: chlorine Cl gases, bromine Br gases, and nitrogen oxides NO_x, each with different concentrations in the atmosphere [4]. Many of these gases are from traditional refrigerants, such as CFCs (Chlorofluorocarbons) and HCFCs (Hydrochlorofluorocarbons) used widely in 1.4 billion air conditioners and 0.7 billion refrigerators in late 20th century in the world [5].

In the 1980s, under the guidance of Prof. Crutzen, scientists Molina and Rowland made a significant discovery through laboratory experiments and computational modeling, and identified a crucial link between chlorofluoromethane and the ozone hole. This significant finding earned them the Nobel Prize in Chemistry in 1995 [6, 7].

The distribution of global stratospheric ozone is influenced by many factors, such as geographical location, altitude, time of day and month of the year, and amounts of different ODSs. The total ozone column above a specific location typically ranges from 200 to 500 DU (Dobson Units), with a global average of 300 DU [1, 7]. The UV beams are mostly strong to generate more atomic oxygen and thus ozone molecules in the tropical areas. However, the total ozone is observed to be lower above the equator and higher in the mid-latitudes and polar region. It is believed due to the gradual, large-scale horizontal circulation of ozone-rich tropical stratospheric air towards the polar zones [1, 6, 8], which contributes to the observed differences in ozone concentrations and profile across different latitudinal zones of Earth.

In studying the atmospheric phenomena, including the ozone layer, researchers have developed different modeling and numerical tools. While 2-D (Two-Dimensional) models have been the primary focus, it is worthy of noting the use of the simpler 1-D models that oftentimes give specific insights and understanding into ozone concentrations, ozone layer in stratosphere, and impacts of various ozone depleting processes [1, 5, 9]. Among the prevailing 2-D models, the 2-D chemical models represent an initial attempt to incorporate the influence of circulation and mixing on changing atmospheric circumstances. Utilizing 2-D grids to depict latitude and altitude, these models broadly capture average conditions across latitude bands as a function of elevation and latitude [10]. While more accurate in consistent circumstances like the high stratosphere, they face limitations in accurately capturing eddy forcing in less homogeneous areas such as the lower stratosphere. Despite these constraints, 2-D models serve as useful tools to understand radiative-chemical interactions and improve spatial distribution knowledge through their simplicity [11].

Zonal mean models, another 2-D approach, divide the atmosphere into latitude bands to calculate average ozone concentrations [12]. Their simplicity makes them computationally efficient and easy to set up, enabling the study of large-scale trends and patterns. However, they have limitations, such as not accounting for regional variations in ozone concentration or the impact of atmospheric circulation patterns [12]. While helpful for analyzing ozone layer behavior, combining zonal mean models with other models and observational data is crucial for a better understanding of dynamics and behavior [13]. NWP (Numerical Weather Prediction) models, designed for weather prediction, have not yet incorporated ongoing chemical changes in the atmosphere [14]. These models consider air and water properties from a physical standpoint, encompassing the transfer of momentum, heat, mass, and humidity in the atmosphere through parameterizations due to computational limitations. Despite their complexity, NWP models lack consideration for chemical alterations in the atmosphere, highlighting the need for further updates to enhance their accuracy in long-term forecasts [15].

In this paper, we aim at contributing to the exploration of ozone distribution and depletion in the stratosphere, taking an engineering approach. Our study employs a system approach based on the conservation of materials of ozone and other species in a cylindrical coordinate system. This methodology is anticipated to enhance prediction accuracy and provide a better understanding of ozone behavior, stratospheric layer, and ozone depletion and holes. Notably, our model diverges from existing literature by incorporating a convection-diffusion-reaction mechanism within a cylindrical coordinate system. This approach gives advantages of faster computation and improved capabilities for solving smaller solution domains, and of focused analyses on specific regions like ozone holes. In this paper, we present our on-going efforts of developing the 2-D model of mass balance equations with various ozone generation and depletion reactions, the validation of our calculated results with the measured data and the analytical results, and the initial finding of latitudinal ozone distributions and depletion of stratospheric ozone.

2. Modeling and Numerical Method

2.1 Mass Balance Equations

In our investigation of ozone distribution, depletion and hole in the stratosphere, we employ a system approach of 2-D mass balance equations in cylindrical coordinates [1, 16]. The conservation equations of a chemical species, including ozone O_3, with concentration C_i account for the change with time ($\frac{\partial C_i}{\partial t}$), convective transport due to slow air movement ($\boldsymbol{U}.\nabla C_i$), mass diffusion due to concentration gradients ($D_i\nabla^2 C_i$), and the impact of various chemical reactions ($\frac{d[C_i]}{dt}$), including photolysis, ozone generation and depletion processes. These coupled partial differential equations governing the dynamic changes of a species in the stratosphere consider five concurrent competing physical-chemical-radiative processes: convective transport, mass diffusion, photo-dissociation, ozone generating reactions, and ozone depleting reactions.

The formulation of equations in cylindrical coordinates with axisymmetric assumption ($\partial C/\partial\phi = 0$) are listed below, where z being the altitude or elevation (from 10 km to 50 km for the stratosphere), r being the radial coordinate, t being the time (in s, day, or month), U_z and U_r being the slow wind speed in z and r directions, and D_i being the mass diffusivities of C_i gas. The concentration C_i (in ppm or in molecules/volume) of species gases can be ozone O_3, atomic oxygen O, regular oxygen molecule O_2, and various ozone depleting chemicals, such as Cl, ClO, Br, BrO, NO, NO_2, etc..

Conservation of mass equations:

$$\frac{\partial C_i}{\partial t} = \frac{1}{r}\frac{\partial}{\partial r}\left[\left(D_i\frac{\partial C_i}{\partial r}r\right) - U_r C_i r\right] + \frac{\partial}{\partial z}\left(D_i\frac{\partial C_i}{\partial z} - U_z C_i\right) + \frac{d[C_i]}{dt}$$

The possibly involved photolysis and chemical reactions for the last term $\frac{d[C_i]}{dt}$ are:

$$O_2 + hv(sunlight) \longrightarrow 2\ O^* \quad (1)$$

$$O^* + O_2 + M \longrightarrow O_3 + M \quad (2)$$

$$O_3 + hv(sunlight) \longrightarrow O_2 + O^* \quad (3)$$

$$\mathrm{Cl} + O_3 \longrightarrow \mathrm{ClO} + O_2 \quad (4)$$

$$\mathrm{ClO} + \mathrm{O} \longrightarrow \mathrm{Cl} + O_2 \quad (5)$$

$$\mathrm{ClO} + \mathrm{ClO} + \mathrm{M} \longrightarrow (\mathrm{ClO})_2 + \mathrm{M} \quad (6)$$

$$(\mathrm{ClO})2 + hv(sunlight) \longrightarrow \mathrm{Cl} + \mathrm{ClOO} \quad (7)$$

$$\mathrm{ClOO} + \mathrm{M} \longrightarrow \mathrm{Cl} + O_2 + \mathrm{M} \quad (8)$$

$$\mathrm{NO} + O_3 \longrightarrow \mathrm{N}O_2 + O_2 \quad (9)$$

$$\mathrm{N}O_2 + \mathrm{O} \longrightarrow \mathrm{NO} + O_2 \quad (10)$$

$$\mathrm{N}O_2 + O_3 \longrightarrow \mathrm{NO} + 2O_2 \quad (11)$$

$$\mathrm{Br} + O_3 \longrightarrow \mathrm{BrO} + O_2 \quad (12)$$

$$\mathrm{BrO} + ClO \longrightarrow \mathrm{BrCl} + O_2 \quad (13)$$

$$BrCl + hv(sunlight) \longrightarrow \mathrm{Br} + Cl \quad (14)$$

Eqs. (1) to (3) represent the Chapman mechanism, introduced in 1930, which delineated the natural processes (without man-made ODSs depletion) of ozone generation and consumption via photo-excitation, collision-induced transformation, and dissociation,

and the non-reactive species (M) being a random stabilizing intermediate, such as N_2 [17]. Throughout the stratosphere, ozone O_3 is formed in multistep chemical processes that are initiated by sunlight (UV radiation), which photo-dissociates the abundant oxygen molecules O_2 into active oxygen atoms O. The atomic oxygen O combines with regular oxygen molecule O_2 to produce ozone O_3. Since concentration of molecular oxygen O_2 is very large and stable at 20.95% (or 2.095×10^5 ppm), the amount of ozone generated depends primarily on the concentration of atomic oxygen O.

Eqs. (4) to (14) represent three possible ozone depleting reaction cycles from man-made ODSs [18]. Eqs. (4) to (8) describe how chlorine-containing chemicals, such as traditional refrigerants CFCs and HCFCs, participate in turning ozone O_3 into oxygen molecule O_2. Chlorine is considered an ozone-depleting reaction catalyst, since the active chlorine gases Cl, ClO, ClOO, and $(ClO)_2$ are reformed after the completion of its respective cycle, which can be used again for further destruction of ozone.

Eqs. (9) to (11) describe how pollutants nitrogen oxides NO_x, such as nitrogen monoxide NO and nitrogen dioxide NO_2, from combustion of fossil fuels or natural processes at Earth surface, can react with ozone O_3 to reduce it to regular oxygen O_2, once it accumulates and transports to the stratosphere by air motion in troposphere. Eqs. (12) to (14) describe how bromine-containing chemicals, such as CH_3Br (Methyl Bromide) and halons, which are a group of industrial compounds containing at least one bromine Br atom, originally developed for fires extinguishing and later also for use in large computer, hardware, and engine protection [7, 18]. Similar to chlorine, bromine can effectively participate in turning ozone O_3 into oxygen molecule O_2. Bromine is also considered an ozone-depleting catalyst, since the active bromine gases Br, BrO, and BrCl are reformed after the completion of its respective cycle and can be re-used.

To investigate the natural generation and depletion of ozone in Eqs. (1) to (3), and man-made catalytic ozone depletion reactions in Eqs. (4) to (14), we use a system of first order ordinary differential equations for the chemical reaction expressions, $\frac{d[\text{ Reactant}]}{dt} = r_i$, or = r_1, r_2, … or r_{14}, as summarized in Table 1. These coupled chemical reaction equations, when plugged into the Mass Balance Equation with transient mass diffusion and convective transport, capture the intricate dynamics and changes of ozone and other species in the

Table 1 The reaction rate constants k_i's, initial concentrations of different species, and reaction expression of Eqs. (1) to (14) [18].

Eq. number	Reaction rate constants (k) $(cm^3/\ molecules * s)$	Initial concentrations (C) $(molecules/cm^3)$	Reaction expression (r)
1	$k_1 = 1.03 \times 10^{-94}$	$O_2 = 2.00 \times 10^{17}$	$r_1 = k_1 [O_2]$
2	$k_2 = 5.92 \times 10^{-34}$	$O = 1.00 \times 10^{-6}$	$r_2 = k_2 [O_2] [O]$
3	$k_3 = 4.38 \times 10^{-26}$	$O_3 = 5.00 \times 10^{12}$	$r_3 = k_3 [O_3]$
4	$k_4 = 1.22 \times 10^{-11}$	$Cl = 6.46 \times 10^4$	$r_4 = k_4 [O_3] [Cl]$
5	$k_5 = 3.80 \times 10^{-11}$	$ClO = 7.22 \times 10^7$	$r_5 = k_5 [O] [ClO]$
6	$k_6 = 2.16 \times 10^{-32}$	$(ClO)_2 = 1.00 \times 10^{-6}$	$r_6 = k_6 [ClO]^2$
7	$k_7 = 8.53 \times 10^{-15}$		$r_7 = k_7 [(ClO)_2]$
8	$k_8 = 6.51 \times 10^{-13}$	$ClOO = 1.00 \times 10^{-6}$	$r_8 = k_8 [ClOO]$
9	$k_9 = 1.78 \times 10^{-14}$	$NO = 1.00 \times 10^9$	$r_9 = k_9 [O_3] [NO]$
10	$k_{10} = 1.05 \times 10^{-11}$	$NO_2 = 1.00 \times 10^9$	$r_{10} = k_{10} [NO_2] [O]$
11	$k_{11} = 1.00 \times 10^{-18}$		$r_{11} = k_{11} [NO_2] [O_3]$
12	$k_{12} = 1.18 \times 10^{-12}$	$Br = 3.2 \times 10^5$	$r_{12} = k_{12} [Br] [O_3]$
13	$k_{13} = 1.02 \times 10^{-12}$	$BrO = 6.4 \times 10^6$	$r_{13} = k_{13} [BrO] [ClO]$
14	$k_{14} = 1.06 \times 10^{-8}$	$BrCl = 1.00 \times 10^{-6}$	$r_{14} = k_{14} [Br] [Cl]$

Table 2 The overall chemical reaction equations for different species $\frac{d[C_i]}{dt}$ in mass balance equation, considering Eqs. (1) to (14), where r_i's are listed in Table 1.

Chemical species	Reaction expression
$\frac{d[O_2]}{dt} =$	$-r_1-r_2+r_3+r_4+r_5+r_8+r_9+r_{10}+2r_{11}+r_{12}+r_{13}$
$\frac{d[O_3]}{dt} =$	$r_2-r_3-r_4-r_9-r_{11}-r_{12}$
$\frac{d[O]}{dt} =$	$2r_1-r_2+r_3-r_5-r_{10}$
$\frac{d[Cl]}{dt} =$	$-r_4+r_5+r_7+r_8+r_{14}$
$\frac{d[ClO]}{dt} =$	$r_4-r_5+2r_6-r_{13}$
$\frac{d[(ClO)_2]}{dt} =$	r_6-r_7
$\frac{d[ClOO]}{dt} =$	r_7-r_8
$\frac{d[NO]}{dt} =$	$-r_9+r_{10}+r_{11}$
$\frac{d[NO_2]}{dt} =$	$r_9-r_{10}-r_{11}$
$\frac{d[Br]}{dt} =$	$-r_{12}+r_{14}$
$\frac{d[BrO]}{dt} =$	$r_{12}-r_{13}$
$\frac{d[BrCl]}{dt} =$	$r_{13}-r_{14}$

stratosphere. Thus, our model allows exploring and quantifying different catalytic cycles of man-made ozone depletion reactions, including chlorine, bromine, and nitrogen oxides under various stratospheric conditions, different times and months of the year, and different geographical locations [19].

Table 1 also lists the detailed reaction rate constants k_i, initial concentrations of different species, and reaction rate expression of Eqs. (1) to (14) [18]. It should be noted that at different latitudinal location, time and months of the year, and special conditions, the data of k_i and initial concentrations in Table 1 would be different. Based on the reaction expression r_i for each equation in Table 1, Table 2 further lists an overall expression of the coupled reaction rate for each species $\frac{d[C_i]}{dt}$ considering reactions in Eqs. (1) to (14), including the changes of ozone concentration from reactions $\frac{d[O_3]}{dt}$, and thereby the profile and peak of ozone layer, and total ozone abundance. For example, in addition to mass diffusion and convective transport, the concentrations of ozone change with the involved chemical reactions of one generation and five consumptions, as $\frac{d[O_3]}{dt} = r_2 - r_3 - r_4 - r_9 - r_{11} - r_{12}$.

2.2 Numerical Methods

With the mass balance equations, we study ozone O_3 behavior and other species across time and space, or $[O_3] = f(t, r, z)$, with axisymmetric assumption ($\partial C_i/\partial\phi = 0$) and under different boundary and initial conditions in the stratosphere. The axisymmetric assumption is to solve in a single plane of r - z, rotating cylindrically, which simplifies the calculations by neglecting polar or azimuthal angle variation, and give acceptable results for a smaller region on the globe and good results for the polar region of different sizes of radius r. We employ finite difference formula to approximate the first- and second-order partial derivatives in spatial (r and z) and temporal (t) dimensions to turn the partial differential

equations into a large system of simultaneous algebraic equation in a specified solution domain [20-22]. The first-order partial derivatives, $\frac{\partial C_i}{\partial t} = \frac{C_{i\ (i,j,n+1)} - C_{i\ (i,j,n-1)}}{2\Delta t}$, $\frac{\partial C_i}{\partial r} = \frac{C_{i\ (i,j+1,n)} - C_{i\ (i,j-1,n)}}{2\Delta r}$, and $\frac{\partial C_i}{\partial z} = \frac{C_{i\ (i+1,j,n)} - C_{i\ (i-1,j,n)}}{2\Delta z}$, and the second-order partial derivatives, $\frac{\partial^2 C_i}{\partial r^2} = \frac{C_{i\ (i+1,j,n)} - 2C_{i\ (i,j,n)} + C_{i\ (i-1,j,n)}}{\Delta r^2}$ and $\frac{\partial^2 C_i}{\partial z^2} = \frac{C_{i(i,j+1,n)} - 2C_{i(i,j,n)} + C_{i(i,j-1,n)}}{\Delta z^2}$ were employed, with discretizing the solution domain into many grid meshes of the chosen Δt, Δr, and Δz in the stratosphere.

The numerical solution process involves the formulation of the time-dependent convection-diffusion partial differential equation, which is applied separately to O_3 (ozone), O_2 (molecular oxygen), O (atomic oxygen), and any species concerned. Since the partial pressure or concentration of molecular oxygen O_2 is very large with a stable amount of 20.95% of air, which is much larger than the changes in concentrations of gases, typically in the order of ppm (10^{-6}), the mass balance equation for molecular oxygen O_2 can be safely dropped because the changes of O_2 will be negligibly small, from various reactions in the stratosphere. With that, we then add the last term, $\frac{d[C_i]}{dt}$, the overall chemical reactions, which are first order ordinary differential equations, as listed in Tables 1 and 2.

A large set of simultaneous finite difference algebraic equations can be systematically set up, as listed below in Eq. (15) for all grid meshes, which consider the mass diffusion due to concentration gradients, transport by advection of air motion, and various involved chemical reactions of both generation and depletion of ozone and other species in the solution domain of hundreds or thousands grid meshes in the stratosphere.

$$
\begin{aligned}
{O_3}^{n+1}{}_{i,j} = {O_3}^{n}{}_{i,j} + \Delta t \\
&* \left\{ \frac{1}{r} \left[\frac{D_i}{\Delta r^2} r \left({O_3}^{n}{}_{i+1,j} \right.\right.\right. \\
&\left. - 2{O_3}^{n}{}_{i,j} + {O_3}^{n}{}_{i-1,j} \right) \\
&+ \frac{D_i}{2\Delta r} \left({O_3}^{n}{}_{i+1,j} - {O_3}^{n}{}_{i-1,j} \right) \\
&- \frac{U_r}{2\Delta r} r \ \left({O_3}^{n}{}_{i+1,j} \right. \\
&\left. \left. - {O_3}^{n}{}_{i-1,j} \right) - U_r {O_3}^{n}{}_{i,j} \right] \\
&+ \left[\frac{D_i}{\Delta z^2} \left({O_3}^{n}{}_{i,j+1} - 2{O_3}^{n}{}_{i,j} \right.\right. \\
&\left. + {O_3}^{n}{}_{i,j-1} \right) \\
&- \frac{U_z}{2\Delta r} \left({O_3}^{n}{}_{i,j+1} \right. \\
&\left. \left. - {O_3}^{n}{}_{i,j-1} \right) \right] \Bigg\} + \Delta t * \frac{d[{O_3}^{n}]}{dt}
\end{aligned}
\tag{15}
$$

where

$$
\begin{aligned}
\frac{d[{O_3}^{n}]}{dt} &= r2 - r3 - r4 - r9 - r11 - r12 \\
&= k2\ [O2]\ [O] - k3\ [O3] \\
&- k4\ [O3]\ [Cl] \\
&- k9\ [O3]\ [NO] \\
&- k11\ [NO2]\ [O3] \\
&- k12\ [Br]\ [O3]
\end{aligned}
\tag{16}
$$

The overall changes of ozone in the stratosphere by various natural and man-made chemical reactions is listed in Eq. (16), which involves one strong generating reaction by natural processes (or photolysis of Chapman mechanism in Eqs. (1) and (2)), and five possible depleting reactions of different degrees. The depletion of ozone includes the natural photo-dissociation in Eq. (3), depletion by chlorine gases in Eq. (4), depletion by NO_x in Eqs. (9) and (11), and depletion by bromine gases in Eq. (12).

For numerical solutions, we implemented the Python Solvers which offer a robust environment for

solving a large system of simultaneous complex equations. Python as our software for code execution, has extensive libraries for numerical computations of large number of equations. We discretize the altitude (elevation) z by Δz = 1 km to 2 km, or the dimensionless altitude z^* = (z-15)/(45-15) or z^* = (z-10)/(50-10), depending on the available measured data to compare to. The dimensionless radial coordinate, $r^* = r/R_{ref}$ and R_{ref} can be selected for a range of 50 km or larger, with discretization of Δr = 1 km to 2 km. The time step Δt was tested with different values from 0.1 s to 10 s for computational convergence, efficiency, and stability, and a better value of Δt = 1 s was selected to capture dynamic changes in ozone concentration with a good temporal resolution. Thus, most our calculated results presented in this paper were conducted with Δt = 1 s, Δz = 2 km or 20 grids along z^* direction (z^* = 0 to 1.0), and also 20 grids along radial direction (r^* = 0 to 1.0).

3. Model Validation

In this study, before we apply our model for calculations of stratospheric ozone concentrations, we will need to validate our 2-D Ozone Model of mass balance equations of ozone and other species with both the Model for various chemical-photolysis reactions and the Model for the convection-diffusion physical processes, separately.

3.1 Chemical-Photolysis Reactions without Convection-Diffusion

We conducted the calculations of transient changes of ozone concentrations without presence of convective transport, nor mass diffusion in the stratosphere. We compared it to the calculated results with depletion by NO_x and CFCs of the well-respected Professor Fogler [16], under the same boundary conditions and rate constants and coefficients. The comparison was also extended to *Kinetics of Ozone Depletion Model* of Chakrabarti et al. [18] under the same conditions, which was a typical stratospheric condition, with transient changes of ozone concentration under catalytic depleting reactions by NO_x and CFCs [18, 21].

Fig. 1 shows a continuous decline in ozone concentration from 5×10^{12} to 0.8×10^{11} molecules O_3/cm^3 over a time period of 7×10^4 s (or 19.5 h). Results of our model (orange curve) follow closely with that of *Kinetics of Ozone Depletion Model* (blue curve) [18]. This good alignment with discrepancy of 3.4% is particularly notable for capturing the complexities of chain reactions involving chlorine, nitrogen oxides, and intermediate species. The continuous decay of ozone with time of reactions in both curves delineates the intricate dynamics of ozone depletion in the stratosphere.

3.2 Convection-Diffusion of Substance without Chemical Reactions

We conducted the calculations of transient changes of a substance, such as ozone in stratosphere, by convection and diffusion, but without chemical-photolysis reactions. We compared our calculated results to the available analytical solutions of 2-D convection-diffusion equation [23].

We used the same *Centered Explicit Finite Difference* method of the referenced paper [23] and carefully compare the respective results. This validation is essential to ensure the reliability of our approach in understanding convection-diffusion processes.

Fig. 2 presents the contour results illustrating the effects of convection and diffusion at 10% of the total simulation time (two upper diagrams), and the resulting distribution at 90% of the simulation time (two lower diagrams). The evolving substance distributions over these time intervals exhibit a good agreement, with a discrepancy of only 0.62% between our computed results and the analytical solutions [23]. This reaffirms the precision of our numerical approach in capturing the convection-diffusion dynamics.

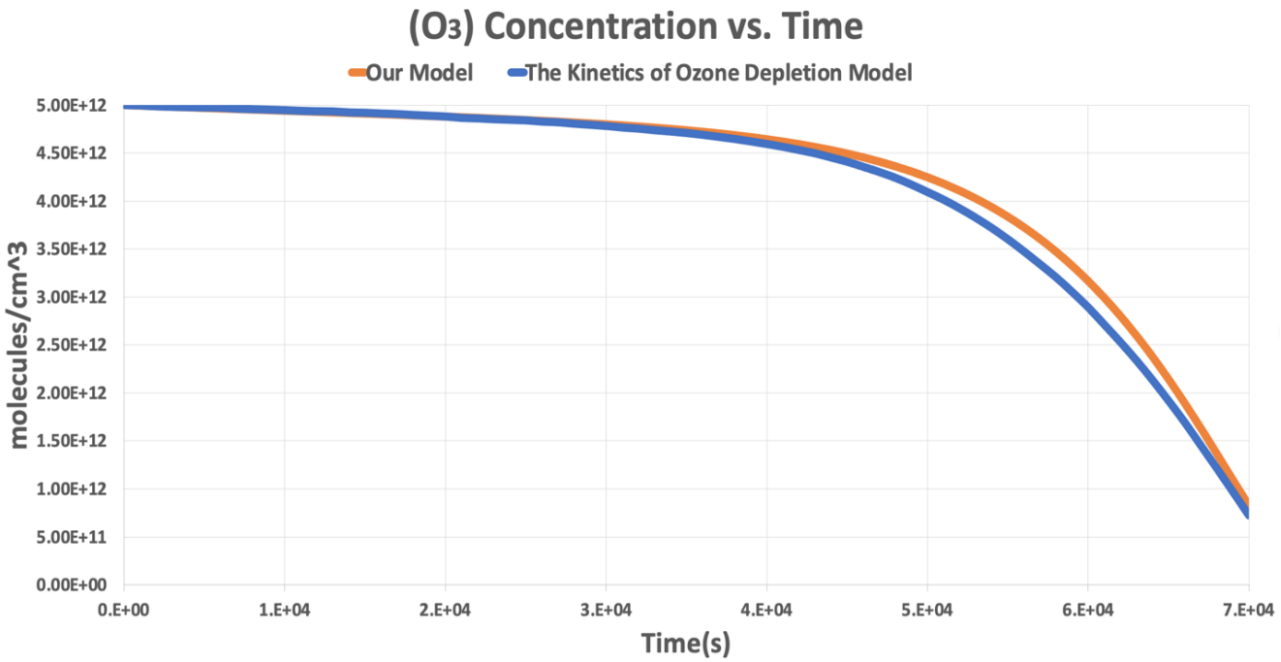

Fig. 1 Comparative analysis of transient change of ozone concentrations and depletion caused by NO_x and CFCs, our model (orange curve) plotted against the Kinetic Ozone Depletion Model (blue curve) [18].

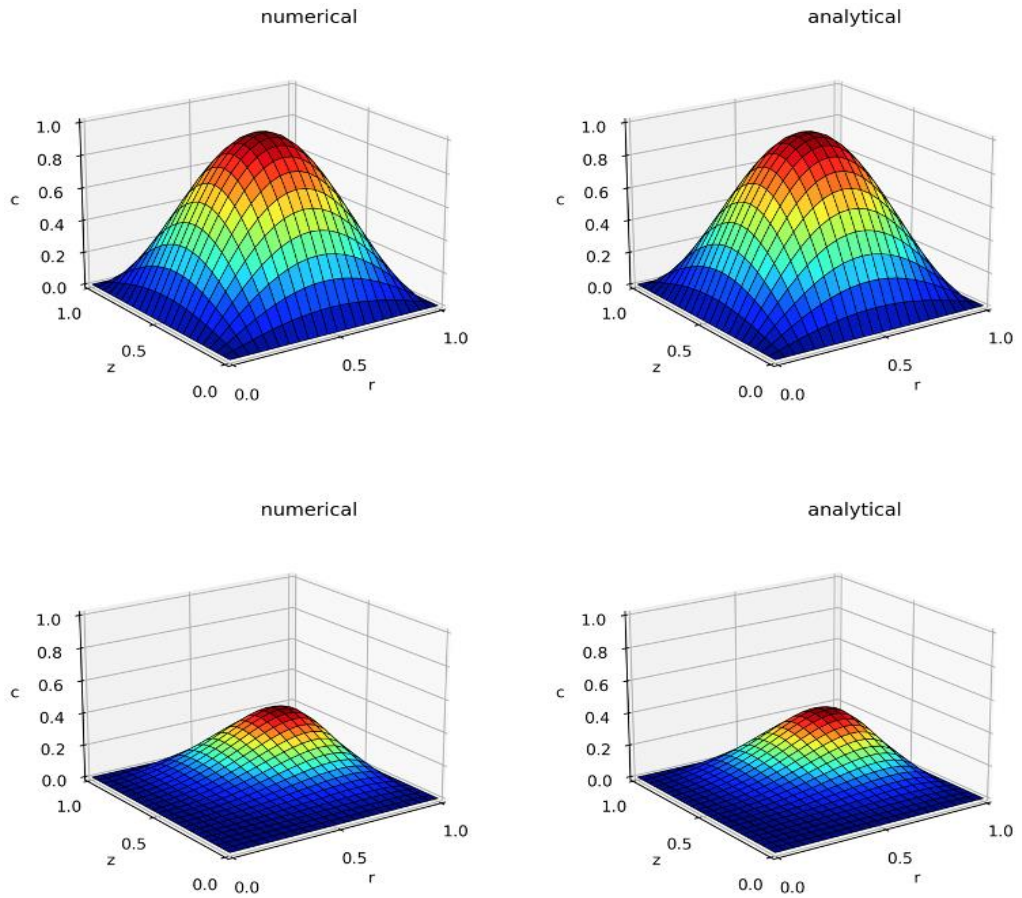

Fig. 2 Comparison of the analytical solutions [23] and our model calculations of transient distribution of a substance by convection and diffusion at 10% of total simulation time (two upper diagrams) and at 90% of total simulation time (two lower diagrams).

4. Results and Discussions

Ozone O_3, a tri-atomic gas naturally occurring in the stratosphere, possesses a distinct pungent odor, detectable even in trace amounts. Its discovery dates back to laboratory experiments in the mid-1800s, while its atmospheric presence was quantified through chemical and optical methods during the mid-1900s [7].

4.1 Calculated Ozone Distributions as Compared to Measured Data

To validate our model against the published measured data [24], we calculated ozone concentrations and distribution at two geographical locations: the Equator (close to Singapore) and mid-latitude 40 ° S (close to Melbourne, Australia). The equatorial region, known for its intense and long radiation from the Sun, provides an ideal setting for unraveling ozone distribution dynamics and their impact by UV radiation levels. On the other hand, the choice of 40 °S allows us to explore ozone distribution under different solar radiation characteristics.

As shown in Fig. 3, the trend of calculated ozone concentrations (dotted red curve) in the equatorial stratosphere exhibited a similar profile to the measured data at the Equator (solid red curve). The average ozone concentration was shown to be less than 1% and the variation of distributions to be less than 14%. As seen in Fig. 3, the actual ozone concentration starts at a low value of 3 ppm near the top boundary of upper stratosphere at z = 45 km, and increases to a maximum value of 9.41 ppm (as compared to the measured value of 9.76 ppm) near the mid-stratosphere around z = 30 km, which indicates the richest layer or the peak of the stratospheric ozone. It decreases to a low value of 0.5 ppm near the bottom boundary of lower stratosphere around z = 15 km, which connects and transitions into the tropopause and troposphere. Fig. 3 also shows the calculated ozone concentrations (dotted gray curve) along the altitude at mid-latitude location of 40 ° S (solid gray curve), which displays a similar profile to the measured data collected by the MLS (Microwave Limb Sounder) ozone instrument [24].

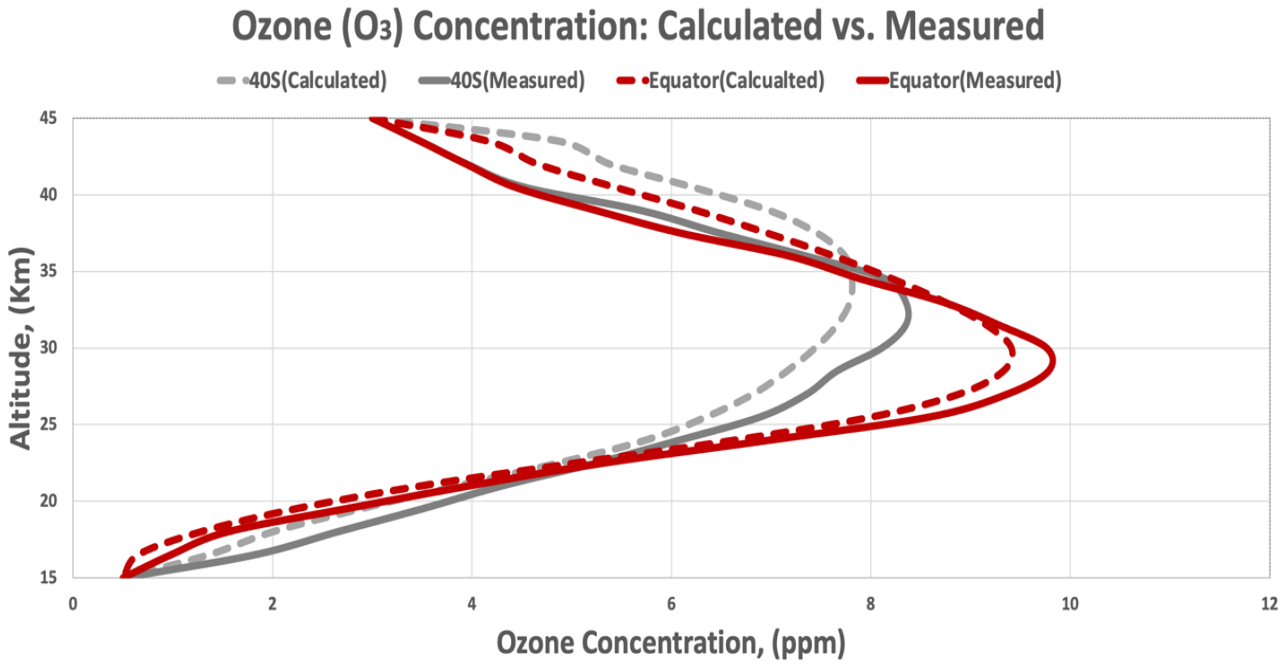

Fig. 3 Comparison of calculated ozone concentrations and distribution (dotted curves) with the measured data (solid curves) at two geographical locations: the Equator (red curves) and 40 °S (gray curves).

In the upper stratosphere of the tropical region, the incoming solar beam, primarily high energy ultraviolet (UV-C and UV-B), initiates the photolysis of molecular oxygen O_2 to turn into two oxygen atoms O, as in Eq. (1). The chemically active atomic oxygen O collides with abundant O_2 to form molecular ozone O_3, as in Eq. (2). As more atomic oxygen is generated by UVs, more ozone will be formed, until the maximal abundance of ozone is reached around mid-stratosphere. As UV radiation penetrates through the stratosphere, it is absorbed with its intensity which deteriorates with the depth of air mass traveled. Meanwhile, as more O_3 is generated with an increased concentration, the ozone-depletion reactions in Eqs. (3), (4), (9), (11) and (12) become increasingly prominent which consumes the formed ozone. In the presence of man-made ozone-depleting chemicals, shown in Eqs. (4), (9), (11) and (12), more ozone will be depleted in an increased rate in the lower part of the stratosphere. Besides the chemical reactions, physical processes of mass diffusion from concentration gradient and convective transport of mild air motion can also change the concentrations and distribution of ozone in the stratosphere.

Table 3 lists the detailed latitudinal changes of calculated ozone concentrations along the altitude in the stratosphere (from 45 km to 15 km) at strategic locations of 90 ° S (the South Pole), 60 ° S (close to Belo Horizonte, Brazil), 40 ° S (close to Melbourne, Australia), 20 ° S (close to Belo Horizonte, Brazil), and 0 ° S (the Equator). For data comparison and model validation, Table 3 also lists the measured data at 40 °S and the Equator [24].

Table 3 Latitudinal changes of calculated stratospheric ozone O_3 concentrations along the altitude in the stratosphere, as compared to the published measured data: Calculated (C) and Measured (M).

Altitude z, km	Ozone concentration, ppm								
	South pole 90 °S	60 °S	40 °S			20 °S	Equator 0 °S		
	(*C*)	(*C*)	(*C*)	(*M*)	$[(C - M)/M]^2$	(*C*)	(*C*)	(*M*)	$[(C - M)/M]^2$
45	3.00	3.00	3.00	3.00	0.00	3.00	3.00	3.00	0.00
43.5	5.19	5.83	4.87	3.48	0.16	4.24	4.16	3.48	0.04
42	5.33	6.12	5.38	3.95	0.13	4.76	4.66	3.94	0.03
40.5	5.59	6.68	6.21	4.52	0.14	5.58	5.43	4.43	0.05
39	5.78	7.04	6.97	5.68	0.05	6.46	6.24	5.23	0.04
37.5	5.71	7.12	7.46	6.48	0.02	7.08	6.96	6.09	0.02
36	5.43	6.96	7.74	7.35	0.00	7.58	7.63	7.18	0.00
34.5	5.15	6.69	7.81	8.15	0.00	8.01	8.22	7.90	0.00
33	4.88	6.41	7.79	8.35	0.00	8.37	8.74	8.72	0.00
31.5	4.61	6.10	7.66	8.35	0.01	8.63	9.16	9.28	0.00
30	4.44	5.88	7.44	8.11	0.01	8.69	9.41	9.76	0.00
28.5	4.39	5.76	7.16	7.66	0.00	8.52	9.33	9.78	0.00
27	4.38	5.67	6.82	7.36	0.01	8.10	8.89	9.37	0.00
25.5	4.33	5.51	6.35	6.89	0.01	7.36	8.01	8.59	0.00
24	4.18	5.19	5.75	6.09	0.00	6.23	6.65	7.00	0.00
22.5	3.86	4.59	4.87	5.25	0.01	4.88	5.05	5.33	0.00
21	3.47	3.89	3.86	4.30	0.01	3.53	3.49	3.97	0.01
19.5	3.12	3.18	2.88	3.50	0.03	2.39	2.23	2.73	0.03
18	2.60	2.45	2.00	2.65	0.06	1.44	1.28	1.55	0.03
16.5	2.03	1.87	1.36	1.82	0.06	0.79	0.65	0.98	0.11
15	0.50	0.50	0.50	0.50	0.00	0.50	0.50	0.50	0.00
Average (ppm)	4.19	5.07	5.42	5.40	0.03	5.53	5.70	5.66	0.02
DU	288	316	335	372		305	323	353	
Coef. of Variation			18.4%				13.6%		

Table 3 shows the average calculated ozone concentration of 5.70 ppm at the equator, closely aligned with the measured 5.66 ppm, and the peak of 9.41 ppm around z = 30 km, closely agreed with the measured 9.76 ppm. Similarly, at 40 ° S, the average calculated ozone concentration of 5.42 ppm, closely aligned with the measured 5.40 ppm, and the peak of 7.81 ppm around z = 34 km, closely agreed with the measured 8.35 ppm. The discrepancy (coefficient of variation) between the calculated and measured ozone concentrations were 13.6% at the Equator and 18.4% at 40 ° S. The trend of variations, the consistency, and accuracy within an acceptable range of the calculated ozone concentrations, distribution and peak of ozone layer as compared to the published measured data showed our theoretical and numerical model for the transient convection-diffusion-photolysis-chemical reactions is validated by measurements and can be used to study the complex ozone dynamics, ozone layer, and ozone depletion in the stratosphere around the globe.

To help provide further information of the variations of total ozone abundance above a specific location, Fig. 4 shows the rapid changes in air temperature, air density, and total pressure along the altitude z in the troposphere (ground to 10-15 km) and stratosphere (10-15 km to ~50 km). Both air densityρ and total air pressure P decrease rapidly as it ascends in the atmosphere. For example: ρ_{Air} = 1.225 kg/m^3, P_{Air} = 101,325 Pa = 1.01 × 10^8 mPa, and T = 15 ℃ at the ground level; ρ_{Air} = 0.4127 kg/m^3, P_{Air} = 2.64 × 10^7 mPa, and T = -50 ℃ at the bottom boundary of the stratosphere at 10 km; ρ_{Air} = 0.018 kg/m^3, P_{Air} = 1.172 × 10^3 mPa, and T = -46.7 ℃ at the peak of the ozone layer in stratosphere around 30 km; and ρ_{Air} = 0.001 kg/m^3, P_{Air} = 76 mPa, and T = -2.5 ℃ at the top boundary of stratosphere at 50 km.

DU is a measure of total atmospheric (both stratosphere and troposphere) ozone abundance above a location on Earth. One DU represents the number of ozone molecules required to create pure ozone of 0.01 mm column thick at the sea level of temperature 0 ℃ and pressure of 101 kPa (or 1 atm). The total ozone abundance in DU at a geological location can be integrated from the weighted average of ozone O_3 concentration curve in ppm over local T, P, and ρ along the altitude z (from 10 km to 50 km), using a working formula [5].

$$DU = \frac{[O_3]_{ppm}\left[(6.022 * 10^{23})(\frac{P}{RT})\right]}{2.69 * 10^{19}}$$

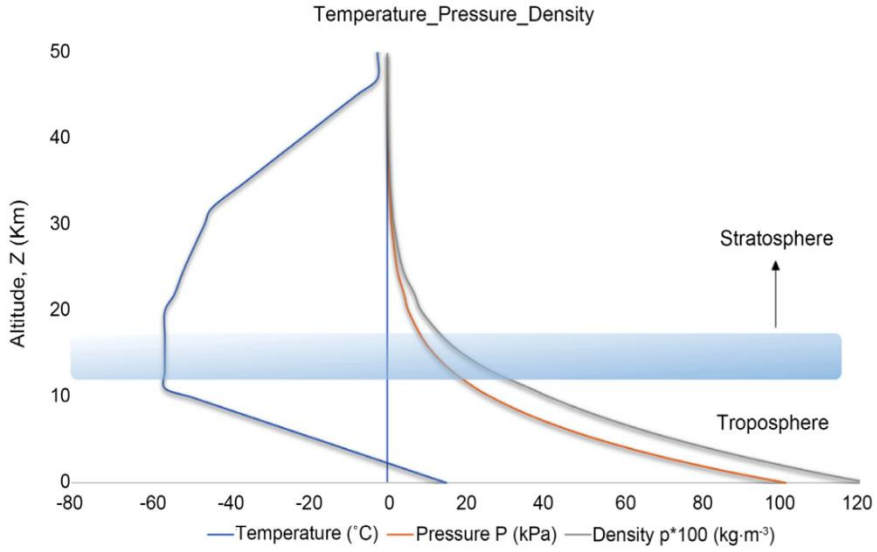

Fig. 4 Rapid changes of the measured air temperature *T*, total pressure *P*, and air density *ρ* along altitude *z* in the troposphere and the stratosphere [1].

As seen in Table 3, the total ozone abundances were calculated to be 335 DU for 40 °S and 323 DU for the Equator, which generally follow, but with less value to, the measured total ozone abundance of 372 DU and 353 DU, respectively. It should be noted here that our calculated ozone abundance is only for the stratosphere (15-45 km), and does not consider the troposphere, which typically accounts for 10% of the total ozone abundance [5 ,7]. This difference explains the slightly lower DU values in our calculations compared to the measurements for both stratosphere and troposphere.

4.2 Latitudinal Variations in Stratospheric Ozone Distribution

In this section, we extend our analysis to a complete calculation of ozone concentrations and distribution at different geographical locations at strategic latitudes, spanning from the Equator to the South Pole. Our objective is to understand the intricate interplay of atmospheric factors that contribute to the observed variations in ozone concentrations. It is noted that the calculated results depend to some extent on the initial and boundary conditions of the published measured ozone and the values of reaction rate constants and gas properties [24], which may not be completely or accurately known. Table 3 lists the detailed values and Fig. 5 plots the trend of distribution of the calculated ozone concentrations in the stratosphere at strategic latitudinal locations from 90 °S (the South Pole), 60 °S, 40 °S, 20 °S, and 0 °S (the Equator). It is noted that the calculated results in Table 3 and Fig. 5 involved about 10 million time steps at Δt = 1 s, extending a period of 4 months, from June to October.

As clearly seen in Fig. 5, under the same or similar convection-diffusion-reactions condition, the profile of ozone concentrations and the peak of the layer shift from 9.41 ppm at 30 km at the Equator (red curve), to 8.69 ppm at 30 km at 20 °S (yellow curve), to 7.81 ppm at 34.5 km at 40 °S (gray curve), to 7.12 ppm at 37.5 km at 60 °S (orange curve), to 5.78 ppm at 39 km at the South Pole (blue curve). These changes happen because of various environmental factors and the chemical equations we use in our model.

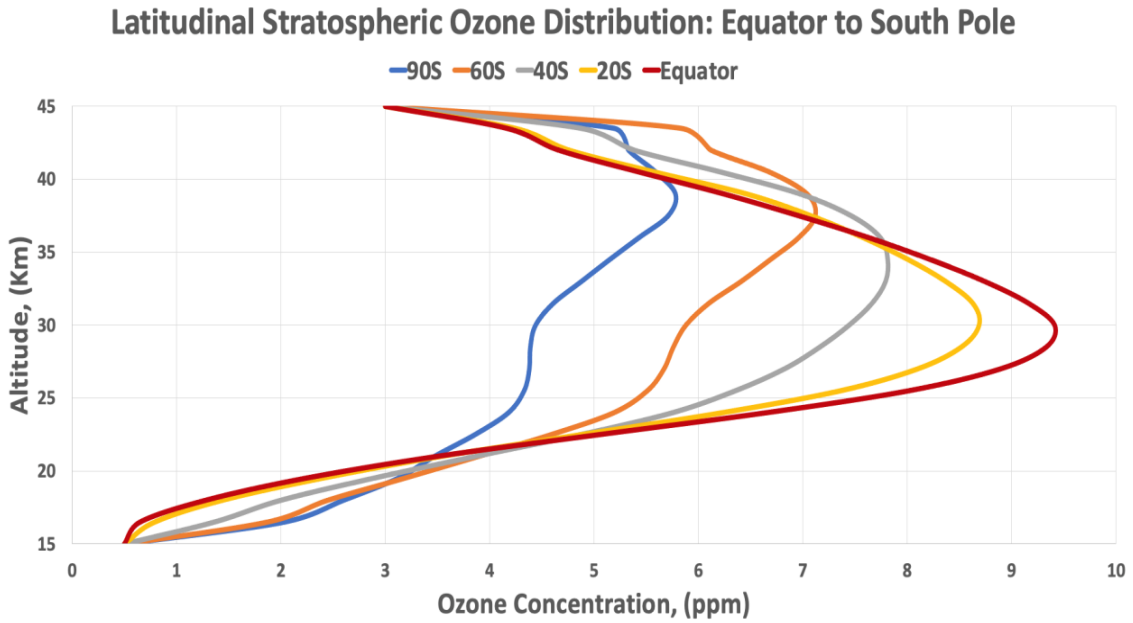

Fig. 5 The trend of ozone distributions of the calculated ozone concentrations in the stratosphere at strategic latitudinal locations from 90 °S (the South Pole), 60 °S, 40 °S, 20 °S, and 0 °S (the Equator), (the calculations involved ~10 million time steps at Δt = 1 s, extending for 4 months from June to October).

Near the Equator, the Sun (with high energy UVs) is known to shine directly overhead, and the tropical region experiences an intense and long sunlight. For the ozone distribution at the Equator (red curve), the strong and long solar (UV) radiation, generates relatively large amount of atomic oxygen O by photolysis of molecular oxygen O_2, and thus more ozone. As UV beam penetrates into the stratosphere, its intensity and ability to generate atomic oxygen deteriorates with the depth of air mass traveled. The ozone concentration (red curve) increases rapidly from 3 ppm at the top of the stratosphere to 9.41 ppm around the mid-stratosphere at 30 km, and decreases rapidly to 0.5 ppm at the bottom of the stratosphere due to the reduced amount of atomic oxygen and increased ozone depletion. The total ozone abundance at the Equator was calculated to be 384 DU.

As we move from the Equator to 20 ° S, 40 ° S, 60 ° S, or 90 ° S (the South Pole), the solar insolation becomes weakened and has an angle. Solar beam penetrates a thicker air mass and less directly reaches to the lower stratosphere, and also with less time duration and smaller intensity. The generation of atomic oxygen by photolysis in Eq. (1) and thereby the ozone production in Eq. (2) are reduced and remain shallow into the air mass of the stratosphere, while the ozone depletion reactions in Eqs. (3), (4), (9), (11) and (12) remain the same. As expected, the peaks of the ozone layer shifted upwards from 30 km to 39 km, and the peak ozone concentrations reduced from 9.41 ppm at the Equator to 5.78 ppm at the South Pole.

Due to the rapid changes of air temperature, pressure, and density along the altitude in the stratosphere, the total ozone abundance in DUs as integrated from the weighted average of ozone concentration curves for 0 ° S (the Equator), 20 ° S, 40 ° S, and 60 ° S remain very steady and stable, from 323 DU, 305 DU, 335 DU to 316 DU, respectively (see Table 3). However, the total ozone abundance at the South Pole is a little smaller at 288 DU, which is a little more than 90% of the average DU for other latitudinal locations. It should be noted that, our 2-D Model for transient dynamics of stratospheric ozone, considering competing processes of convective transport, mass diffusion, photolysis, ozone-depletion reactions, shows good agreement with the published measurement data, and is efficient, and executable to study the complex ozone phenomena in the stratosphere.

5. Summary

To better understand and quantify the dynamics of ozone concentrations, distribution, peak of the layer, total abundance, and ozone depletion, an engineering system approach of 2-D cylindrical model for transient mass balance calculations with all potential (fourteen) photolysis, ozone generating and depleting chemical reactions considered for the stratospheric ozone under different conditions was developed, validated, and tested. The calculated ozone concentrations and profile along the altitude at both the Equator and mid-latitudinal location at 40 ° S were found to exhibit a similar and close profile of the published measured data. The discrepancy between the calculations and measurements for the average ozone concentration was shown to be less than 1% and the variation of distributions to be less than 19%.

Under the same convection-diffusion-reactions condition, the profile of ozone concentrations and the peak of the layer shift from 9.41 ppm at mid-altitude of z = 30 km at the Equator, to 7.81 ppm at z = 34.5 km at 40 ° S, to 5.78 ppm at higher altitude z = 39 km at the South Pole. Near the Equator, the Sun is known to shine directly overhead to give an intense and long UV radiation, which photolysis more atomic oxygen O and generates more ozone. As UV beam penetrates into the stratosphere, its intensity and ability to generate atomic oxygen deteriorates with the depth of air mass traveled. Moving towards 20 ° S, 40 ° S, 60 ° S, or 90 ° S, the solar insolation further becomes weakened with an angle of incidence. Its rays

penetrate a thicker air mass and reaches to the lower stratosphere with less time and smaller intensity. As expected, the peaks of the ozone layer shifted upwards from 30 km to 39 km, and the peak ozone concentrations reduced from 9.41 ppm at Equator to 5.78 ppm at the South Pole.

The total ozone abundances are integrated from the weighted area of ozone concentration curves with the altitude (z) axis, which for the Equator, 20 ° S, 40 ° S, and 60 ° S were found very steady and stable, from 305 DU to 355 DU. However, the total ozone abundance at the South Pole is a little smaller at 288 DU, which is a little more than 90% of the average DU for other latitudinal locations. The calculated total ozone abundance in the stratosphere was found to match well with the measured total ozone abundance, if the ozone in troposphere (10% of total) is deducted.

In summary, this paper presents a robust 2-D Model for analyzing dynamics of stratospheric ozone, considering many competing processes of convective transport, mass diffusion, photolysis, ozone-depletion reactions. The calculated results were validated in good agreement with the published measurement data. This model is convenient, efficient, and executable to study the complex ozone phenomena in the stratosphere.

Acknowledgements

The authors would like to thank the insightful discussions with colleagues of the Catholic University of America's Climate Change Initiatives of Engineering Center for Care of Earth.

References

[1] Wei, L., Alelmi, I., and Nieh, S. 2023. "Calculations of Stratospheric Ozone and Effects of Diffusivity." *Atmospheric and Climate Sciences* 13 (3): 385-400. doi: 10.4236/acs.2023.133021.

[2] United States Environmental Protection Agency (EPA). 2019. "Ozone Layer Protection." Accessed March 10, 2019. https://www.epa.gov/ozone-layer-protection.

[3] Anwar, F., Chaudhry, F., Nazeer, S., Zaman, N., and Azam, S. 2016. "Causes of Ozone Layer Depletion and Its Effects on Human." *Atmospheric and Climate Sciences* 6: 129-34.

[4] Earth System Research Laboratory. 2019. "The NOAA Ozone Depleting Gas Index: Guiding Recovery of the Ozone Layer." Accessed November 20, 2019. https://www.esrl.noaa.gov/gmd/odgi/.

[5] Wei, L., Alelmi, I., and Nieh, S. 2024. "Effects of Chlorine and Chlorine Monoxides on Stratospheric Ozone Depletion," *Atmospheric and Climate Sciences*, Vol. 14, No.1, pp. 136-153. doi: 10.4236/acs.2024.141009.

[6] Molina, M. J., and Rowland, F. S. 1974. "Stratospheric Sink for Chlorofluoromethanes: Chlorine Atom-Catalysed Destruction of Ozone." *Nature* 249 (5460): 810-2.

[7] Salawitch, R. J., Fahey, D. W., Hegglin, M. I., McBride, L. A., Tribett, W. R., and Doherty, S. J. 2019. "Twenty Questions and Answers about the Ozone Layer: 2018 Update—Scientific Assessment of Ozone Depletion: 2018." World Meteorological Organization, etc. Geneva, Switzerland.

[8] Newman, P. A., and Lait, L. R. 2023. "NASA Ozone Watch—Images, Data, and Information for Atmospheric Ozone." NASA-Goddard Space Flight Center, Greenbelt, MD, 2023. https://ozonewatch.gsfc.nasa.gov/Scripts/big_image.php?date=2023-05-18&hem=S&section=HOME.

[9] Steed J. M., Owens A. J., Miller C., Filkin D. L., and Jesson J. P. 1982. "Two-Dimensional Modelling of Potential Ozone Perturbation by Chlorofluorocarbons." *Nature* 295 (5847): 308-11. doi: 10.1038/295308a0.

[10] Vupputuri, R. K. R. 1989. "2-D Model Simulations of Anomalous Spring Variations of Ozone, Temperature and Other Minor Trace Constituents in the Southern Polar Region." *Atmosphere-Ocean* 27 (4): 728-38. doi: 10.1080/07055900.1989.9649364.

[11] Grooß, J., Brühl, C., and Peter, T. 1998. "Impact of Aircraft Emissions on Tropospheric and Stratospheric Ozone. Part I: Chemistry and 2-D Model Results." *Atmospheric Environment* 32 (18): 3173-84. https://doi.org/10.1016/S1352-2310(98)00016-8.

[12] Holton, J. R., and Wehrbein, W. M. 1980. "A Numerical Model of the Zonal Mean Circulation of the Middle Atmosphere." *Pure Applied Geophysics* 118 (1): 84-306. doi: 10.1007/BF01586455..

[13] Waugh, D. W., Oman, L., Newman, P. A., et al., 2009. "Effect of Zonal Asymmetries in Stratospheric Ozone on Simulated Southern Hemisphere Climate Trends." *Geophysics Research Letter* 36 (18): L18701. https://doi.org/10.1029/2009GL040419.

[14] Coopmann, O., Fourrié, N., and Guidard, V. 2022. "Analysis of MTG-IRS Observations and General

Channel Selection for Numerical Weather Prediction Models." *Quarterly Journal of the Royal Meteorological Society* 148 (745): 1864-85. https://doi.org/10.1002/qj.4282.

[15] Balashov, N. V., Thompson, A. M., and Young, G. S. 2017. "Probabilistic Forecasting of Surface Ozone with a Novel Statistical Approach." *J. Applied Meteorological Climatology* 56 (2): 297-316. doi: 10.1175/JAMC-D-16-0110.1.

[16] Fogler, H. S. 2006.*Elements of Chemical Reaction Engineering* (4th ed.). Upper Saddle River, NJ: Pearson International Edition. Prentice-Hall International Series in the Physical and Chemical Engineering Sciences.

[17] Chapman, S. 1930. "A Theory of Upper Atmospheric Ozone." *Memoirs of the Royal Meteorological Society*3: 103.

[18] Chakrabarti, A. K., De Obeso, A., Gürmen, N. M., and Fogler, H. S. 2021. "The Kinetics of Ozone Depletion." Accessed February 8, 2021. http://websites.umich.edu/ ~elements/6e/web_mod/ozone/index.htm.

[19] Brune, W. H. 1998. "Stratospheric Chemistry: Perspectives in Environmental Chemistry." In *Perspectives in Environmental Chemistry*, edited by D. L. Macalady. New York: Oxford Univ. Press, pp. 292-324. https://personal.ems.psu.edu/~brune/m532/meteo532_ch7 _stratospheric_chemistry.htm.

[20] Salman, A. K., Pouyaei, A., Choi, Y., Lops, Y., and Sayeed, A. 2022. "Deep Learning Solver for Solving Advection-Diffusion Equation in Comparison to Finite Difference Methods." *Communications in Nonlinear Science and Numerical Simulation* 115: 106780.

[21] Brasseur, G., and Soloman, S. 1986. *Aeronomy of the Middle Atmosphere.* Dordrecht Holland: D. Reidel Publishing Company.

[22] Claudia, M., and Estaner, R. 2015. "Numerical Simulation by Finite Difference Method of 2D Convection-Diffusion in Cylindrical Coordinates." Accessed December 5, 2021. https://www.researchgate.net/publication/306318916_Numerical_simulation_by_finite_difference_method_of_2D_convection-diffusion_in_cylindrical_coordinates.

[23] Buckman, N. M. 2016. "The Linear Convection-Diffusion Equation in Two Dimensions." Massachusetts Institute of Technology Course 18.303 Linear Partial Differential Equations.

[24] Tang, Q., Prather, M. J., Hsu, J., Ruiz, D. J., Cameron-Smith, P. J., Xie, S., and Golaz, J. C. 2016. "Evaluation of the Interactive Stratospheric Ozone (O3v2) Module in the E3SM." *Geoscientific Model Development* 14: 1219-36. https://doi.org/10.5194/gmd-14-1219-2021.